Nuclear Science and Techniques (2025) 36:137
https://doi.org/10.1007/s41365-025-01708-1

Plan for a super η factory at Huizhou accelerator complex

Xurong Chen[1,2] · Xiong-Hong He[1,2] · Qiang Hu[1,2] · De-Xu Lin[1,2] · Yang Liu[1,2] · Hao Qiu[1,2] · Xu Sun[1,2] · Ye Tian[1,2] · Rong Wang[1,2] · Hong-Lin Zhang[1,2] · Ya-Peng Zhang[1,2] · Cheng-Xin Zhao[1,2]

Received: 17 July 2024 / Revised: 21 October 2024 / Accepted: 28 October 2024 / Published online: 2 June 2025

Abstract
As an approximate Goldstone boson with zero quantum number and zero standard model charge, the long-lived η meson exhibits the decay processes that offer a unique opportunity to explore physics beyond the standard model and new sources of charge parity violation. Further, they facilitate the testing of the low-energy quantum chromodynamics theory and measurement of the fundamental parameters of light quarks. To pursue these goals, we propose a plan to construct a super η factory at HIAF high-energy terminal or at CiADS after its energy upgrade. The high-intensity proton beam at HIAF enables the production of many η samples, exceeding 10^{13} events per year during the first stage, utilizing multiple layers of thin targets composed of light nuclei. This paper presents the physics goals, the first-version conceptual design of the spectrometer, and preliminary simulation results.

Keywords High-intensity frontier · Eta meson factory · New physics · Symmetry breaking · Strong interaction · Silicon-pixel detector

1 Introduction

The high-luminosity frontier presents one approach to new physics [1], as any small deviations from the standard model (SM) predictions in high-precision measurements have implications for new physics beyond the SM. In the next decade, emerging high-intensity proton accelerators will offer a unique opportunity in the exploration for new physics at an unprecedented level. Indications of new physics have been increasingly reported in the literature, for example, the anomalous muon magnetic moment $(g-2)_\mu$ [2–4], X17 boson from the decay of the excited state of ^{8}Be [5–7], lepton flavor universality violation in bottom quark decays [8–12], excesses of cosmic positrons and electrons [13–16], narrow γ ray emissions from the galactic bulge [17], and unexplored nature of dark matter [18–22] and dark energy [23–27]. To date, no evidence of new physics has been observed in the high-energy frontier examined using the large hadron collider. Therefore, some researchers have argued that the new physics of the hidden sector is at low energies [28, 29]. However, the hidden sector is faintly coupled with the SM, making it elusive. For example, the production rates of the light portal particles bridging the hidden and SM sectors are several orders of magnitudes higher at low energies [28]. Moreover, in low-energy, fixed-target experiments, the use of thick targets allows for considerably higher luminosities.

The η meson is of particular interest because it approximates a Goldstone boson arising from spontaneous chiral symmetry breaking and has zero SM charge [30]. Many strong and electromagnetic decay channels of η are forbidden at the leading order; this enhances the rare decay channels of η meson that are sensitive to new physics. Consequently, the η meson serves as an excellent low-energy laboratory for exploring new physics beyond the SM by observing the dark portal particles from η decays [28, 29, 31] or measuring small discrete symmetry breaking such as charge parity (CP) violation and charged lepton flavor violation [32,

This work was supported by the National Natural Science Foundation of China (Nos. 12222512 and 12005266) and the Strategic Priority Research Program of Chinese Academy of Sciences (No. XDB34030300).

✉ Rong Wang
rwang@impcas.ac.cn

[1] Institute of Modern Physics, Chinese Academy of Sciences, Lanzhou 730000, China

[2] School of Nuclear Science and Technology, University of Chinese Academy of Sciences, Beijing 100049, China

33]. A thorough review on the theoretical developments in η and η' decays has recently been reported [32], with regard to high-precision tests of fundamental physics. The latest theoretical models predict four types of portals: vector portal [34–37], scalar portal [38–44], axion-like portal [45–49], and heavy neutral lepton portal [50–52]. Portal particles are particularly significant in theories that seek to bridge the dark and SM sectors. All these light portal particles can be examined by observing the rare decays of η mesons [31, 32]. Symmetry and symmetry breaking form the core of modern physics. Identifying new sources of CP violation is essential for explaining the baryon–antibaryon asymmetry in the universe. Any charged lepton flavor violation is a strong indication of physics beyond the SM model. Several η decay channels facilitate precise testing of these symmetry breakings. Precise measurements of η decay channels are critical in the efforts to elucidate the charge conjugation (C), parity (P), time reversal (T), CP, and charged lepton flavor violations.

In addition to the exploration for new physics, the high-precision study of η decay provides a unique method for testing the quantum chromodynamics (QCD) theory at low energies [53–58], probing the η structure [59–65], precisely measuring the mass difference of light quarks [66–71], and verifying axial anomalies [72–74]. The electromagnetic decay channels associated with virtual and real photons help constrain the η transition form factor with significantly smaller uncertainties [59–64]; this aids the elucidation of the muon anomalous magnetic moment [2–4]. Quark masses are the fundamental parameters of the SM. As regards experimentally constraining light quark masses, the measurement of the isospin-breaking 3π decay channels of η presents a crucial method. High-precision measurements at a super η factory can reduce the uncertainties of QCD parameters significantly. Precise measurements of some rare η decays facilitate the testing of the chiral perturbation theory at high orders [75], which is a rigorous and effective theory for strong interactions at low energies.

As η meson decays involve a wide array of physics phenomena, measurements of η decay have been conducted at facilities worldwide. First, the hadronic generation of η from fixed-target experiments, such as the WASA-at-COSY experiment [76–78] and LHCb experiment [79, 80], has been reported. The WASA-at-COSY collaboration entailed the use of the proton beam at COSY and an internal pellet target, and the number of η event yields on the order of 10^8. Second, the radiative decay of ϕ and J/ψ at the electron–positron colliders have produced considerable numbers of η samples, aided by low-background levels. The number of η events from ϕ decay by the KLOE collaboration is on the order of 10^8 [81–84], while the corresponding number from J/ψ decay by the BESIII collaboration is on the order of 10^7 [85–89]. Third, photoproduction experiments provide a clean environment for the production of η mesons, for example, the A2 experiment at MAMI [59, 90, 91] and the JLab Eta Factory (JEF) [32, 92], which exploit the Primakoff effect [93]. JLab has a long history of studying neutral-meson physics via the Primakoff reaction [94, 95]. In the JEF experiment, approximately 10^9 tagged η events will be collected over the years by using the GlueX spectrometer [96, 97]. Owing to the high-performance calorimetry and high-energy incident photons (up to 11 GeV), remarkable background suppression is achieved for the neutral decay channels. The JEF experiment facilitates the precise measurement of the neutral decay channels of η mesons.

To harness the intriguing discovery potential of light dark portal particles and perform rigorous tests of the SM, it is imperative to build a super η factory using high-intensity accelerators to obtain unprecedented η meson samples. To pursue a vast number of η events, the Rare Eta Decays To Observe Physics beyond the standard model (REDTOP) experiment [31] was proposed in the 2021 US Community Study on the Future of Particle Physics using novel detection techniques. In China, a High-Intensity heavy-ion Accelerator Facility (HIAF) is under construction in Huizhou city by Institute of Modern Physics (IMP), Chinese Academy of Sciences (CAS), which is competitive in the beam intensity. Using this near-future infrastructure, we propose a super η factory at the HIAF high-energy terminal. Undoubtedly, the proposed Huizhou η factory will generate many impactful results that will remarkably advance accelerator and detector technologies.

The remainder of this paper is organized as follows. The proposed Huizhou η factory and its physics goals are described in Sect. 2. The conceptual design of the spectrometer is presented in Sect. 3. Some preliminary simulation results for some golden channels of the experiment are presented in Sect. 4. In Sect. 5, a concise summary and future outlooks are provided.

2 Huizhou η factory and its goals

The HIAF is a major national science infrastructure facility under construction in Huizhou City, Guangdong province, China. in Southern China [98–100]. The construction of the HIAF began in December 2018, and it will be ready for commissioning by the end of 2025. The HIAF is an accelerator complex mainly consisting of a superconducting electron–cyclotron–resonance ion source, continuous-wave superconducting ion linac, booster synchrotron, high-energy fragment separator, and high-precision spectrometer ring. The layout of HIAF is shown in Fig. 1. Many terminals have been designed alongside the accelerator complex for experiments and applications. With high-intensity technology, HIAF not only provides powerful infrastructure for frontier studies in nuclear, high energy-density, and atomic

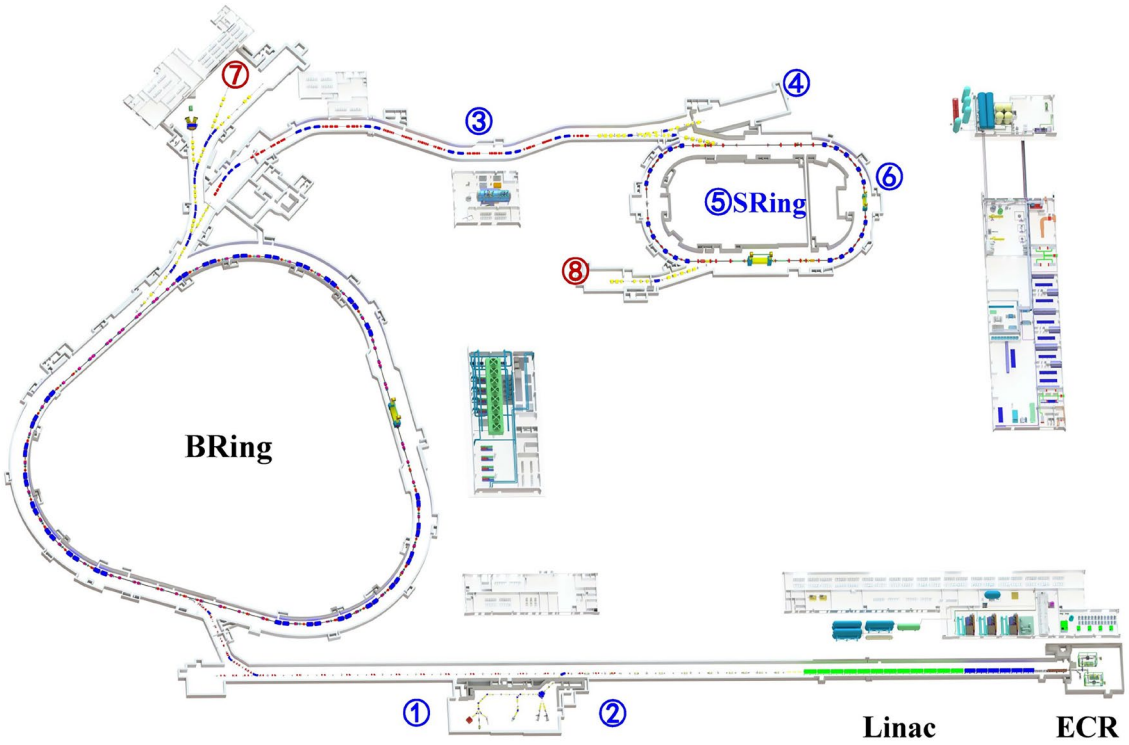

Fig. 1 (Color online) Layout of the HIAF facility. The number "⑦" indicates where the high-energy multidisciplinary terminal is located

physics but is also an excellent platform for heavy-ion applications in life, material, and space sciences [100]. HIAF will potentially deliver unprecedentedly intense ion beams from hydrogen to uranium with energies up to GeV/u. The maximum energy of the proton beam is 9.3 GeV [98–100]. Using heavy-ion beams, HIAF provides an extraordinary platform for studies of hypernuclei and the phase structure of high-density nuclear matter. Further, given its capability to generate high-energy proton beams, HIAF provides an excellent opportunity to study light hadron physics and to build an η factory.

At HIAF, the intensity of the proton beam is higher than 10^{13} ppp (particles per pulse), and the kinematic energy of a proton can reach 9 GeV through the acceleration of the ion linac and booster ring [98–100]. The pulse rate is approximately several Hertz. It is suggested that a super η factory be built at the high-energy multidisciplinary terminal after the booster ring, the terminal "⑦" shown in Fig. 1. The target is made of multiple light-nuclei foils (^{7}Li or ^{9}Be) with 1 cm gaps, significantly reducing the coincident background from the same vertex with no simultaneous decrease in the luminosity. Using a proton beam and light nuclear target, the η meson is efficiently produced with a controlled background at HIAF. The beam-energy thresholds are 1.26 GeV and 2.41 GeV for generating η and η', respectively. Proton–proton scattering at a beam energy of 1.8 GeV results in a large η meson cross-sections [101–104], as indicated by previously reported COSY data (approximately 100 μb) [101]. In the case of the nuclear target, the η meson cross-section is even higher. The HIAF beam intensity and a 1-cm-thick lithium target lead to luminosities above $10^{35}\mathrm{cm}^{-2}\mathrm{s}^{-1}$ for the Huizhou η factory experiment. Regardless of the detector and data acquisition system capabilities, the η production rate can be higher than $10^{8}\ \mathrm{s}^{-1}$ on a light nuclear target ($> 10^{15}$ per year).

The China Initiative Accelerator Driven Sub-critical System (CiADS) is another high-intensity proton accelerator designed for verifying the principle of nuclear waste disposal [105–110]. It provides a remarkably powerful continuous proton beam. The designed full power of the CiADS accelerator is 2.5 MW, with a beam intensity of 3.15×10^{16}pps. CiADS is also appropriate for building a super η factory, provided the energy of CiADS is upgraded to approximately 2 GeV. Because an upgrade to the CiADS accelerator is anticipated to require several years, the HIAF high-energy terminal is deemed more appropriate for the proposed Huizhou η factory.

At the Huizhou η factory, the number of η meson samples is expected to be significant, approximately four orders of magnitude greater than that of the current η events achieved worldwide. With such an enormous yield of η mesons, the main physical goals of the Huizhou η

factory would be to discover new physics by searching for new particles and discrete symmetry breaking and to study SM with extremely high precision. New particles of interest emerging from η and η' decays are the predicted light portal particles below the GeV level, which faintly bridges the SM sector with the hidden sector. Examples include the dark vector particles [34–37], dark scalar particles [38–44], and axion-like particles [45–49]. The protophobic X17 boson of the fifth force [5–7] can also be studied via rare η decay. The remarkably large number of η mesons affords a good opportunity to study new sources of CP violation, which is essential for the matter–antimatter asymmetry in the universe, and to search for charged lepton flavor violation, which is a clear and strong indication of new physics. Finally, precise η decay measurements are critical for high-precision study of the SM, such as strictly constraining the light quark mass difference, precise measurement of meson structure, and high-precision testing of chiral perturbation theory. The primary physics interests are listed in Table 1. As the spectrometer at the Huizhou η factory is particularly suitable for measuring charged particles, the charged decay channels must be attributed a high priority for the proposed experiment, for example, $\eta \to \pi^+\pi^-\pi^0$, $\eta \to e^+e^-\gamma$, $\eta \to \pi^+\pi^-e^+e^-$, and $\eta \to e^+e^-$.

Table 1 List of the main physics goals of Huizhou η factory

Physics goals		Decay channel
New physics	Dark photon & X17	$e^+e^-\gamma$
	Dark Higgs	$\pi^+\pi^-\pi^0$
		$\pi^0e^+e^-$
	Axion-like particle	$\pi^+\pi^-e^+e^-$
		$\pi^+\pi^-\gamma\gamma$
	CP violation	$\pi^+\pi^-\pi^0$
		$\pi^+\pi^-e^+e^-$
	Lepton flavor violation	$\gamma\mu^+e^-$ / c.c
		μ^+e^- / c.c
Precision test of the SM	η transition form factor	$e^+e^-\gamma$
		$e^+e^-e^+e^-$
		$\pi^+\pi^-\gamma$
	Light quark masses	$\pi^+\pi^-\pi^0$
		$\pi^0\pi^0\pi^0$
	Chiral anomaly	$\gamma\gamma$
		$\pi^+\pi^-\gamma$
	Beyond SM weak decay	e^+e^-
	Test chiral perturbation theory	$\pi^+\pi^-\gamma\gamma$
		$\pi^0\gamma\gamma$

3 A compact and large-acceptance spectrometer with silicon pixels

With the rapid development of monolithic silicon pixel technology [111], we developed the concept of a large acceptance and compact spectrometer with silicon pixels to detect the final-state particles at a high event rate. The current design of the spectrometer comprises four main parts: tracking system for charged particles made of silicon pixels, time-of-flight detector for particle identification made of silicon low-gain avalanche detector (LGAD), electromagnetic calorimeter (EM calorimeter) for photon measurement made of lead glass [112], and superconducting solenoid. The 3D design of the spectrometer is shown in Fig. 2. Because of the high granularity and low position resolution of the silicon pixel detector, it is a compact spectrometer with a small volume. Therefore, the EM calorimeter and solenoid are of small size, which reduces the cost of spectrometer fabrication. The inner radius of the superconducting solenoid is approximately 70 cm, and all the main detectors are within the solenoid.

The multi-layer target is placed inside the spectrometer close to the entrance such that there is a large acceptance for fixed-target experiments. Using the current conceptual design of the spectrometer, all forward particles except small-angle particles are covered without dead zones.

To achieve a high-rate capacity for the silicon pixel tracker, the silicon detector group attempted dual

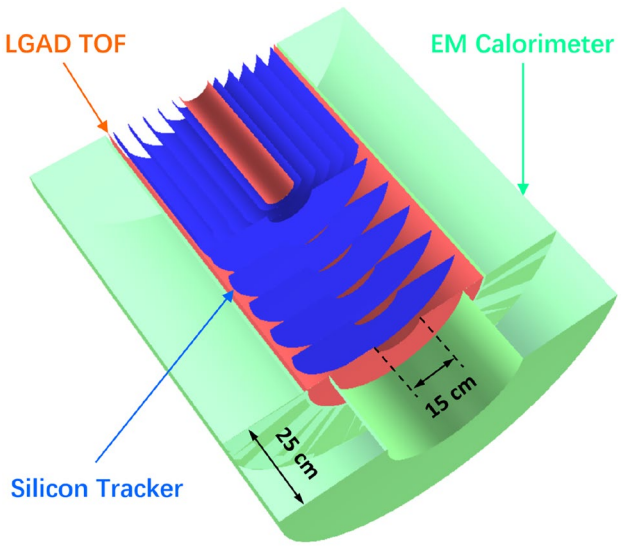

Fig. 2 (Color online) The conceptual design of a compact spectrometer for the η factory. The spectrometer mainly relies on silicon detector technology, with the monolithic silicon pixel tracker and fast LGAD TOF detector of low material budget. The silicon tracker is wrapped with a fast lead-glass calorimeter for high-energy photons

measurements of the energy and arrival time of each pixel [113–117]. Using different arrival times, hits from different events can be distinguished. The objectives of future silicon pixel chips are a resolution of 1–5 ns for arrival time, pixel size of 40–80 µm, and scan time of 100 µs for approximately 100k pixels. In the future, we will reduce the average dead time for one pixel after being hit down to 5–10 µs. The anticipated noise for deposited energy measurement will be around 100 e^-, which is less than 1/5 of the minimum-ionized-particle energy deposition. Under the particle multiplicity of the Huizhou η factory and with the pixel chip more than 5 cm away from the interaction point, the designed silicon pixel chip can easily record events at a rate greater than 100 MHz.

In the current conceptual design of the spectrometer, the calorimeter material is lead glass, which generates only prompt Cherenkov photons. Therefore, it has good time resolution around 100 ps for particle detection. Simultaneously, lead glass is not sensitive to the hadronic shower initiated by nucleons and pions, which means that it has low efficiency for the neutron background and offers additional hadron background suppression capability. Our Geant4 simulation [118–120] discovered that low-energy neutrons ($E_k < 0.3$ GeV) generate almost no hits in the lead glass calorimeter, and a high-energy neutron ($E_k > 1$ GeV) has only approximately 45% probability of depositing more than 10 MeV energy in the calorimeter. As most neutrons from $pA \to X$ collision are low-energy neutrons, the neutron background in photon measurements can be eliminated effectively with the lead glass calorimeter. For inelastic events generated with the GiBUU package [121–124], Fig. 3 shows the invariant mass distributions of two photons, with and without the neutron background. The background of the π^0 signal due to neutron contamination is negligible, especially for the channel $p^7Li \to \pi^+\pi^-\pi^0 X$. In the simulation, the threshold for a hit in the calorimeter corresponds to the signal generated by a 50-MeV photon. Neutrons deposit less energy in the calorimeter than photons, and with the same amount of energy deposition, the hadronic shower initiated by the neutron generates fewer Cherenkov photons. Therefore, the abundant neutron background at low energy is strongly suppressed in the measurement of photons and π^0.

Although a lead glass calorimeter is effective at suppressing hadron backgrounds and is cost-effective, it has significant drawbacks compared to conventional crystal calorimeters. First, the low Cherenkov light yield and severe light attenuation of lead glass result in poor energy resolution. Lead fluoride crystals, which exhibit less light attenuation, can be used instead, but they are much more expensive. Another disadvantage is poor radiation resistance. Although radiation-resistant lead glass can be used to improve this, it suffers from worse light attenuation.

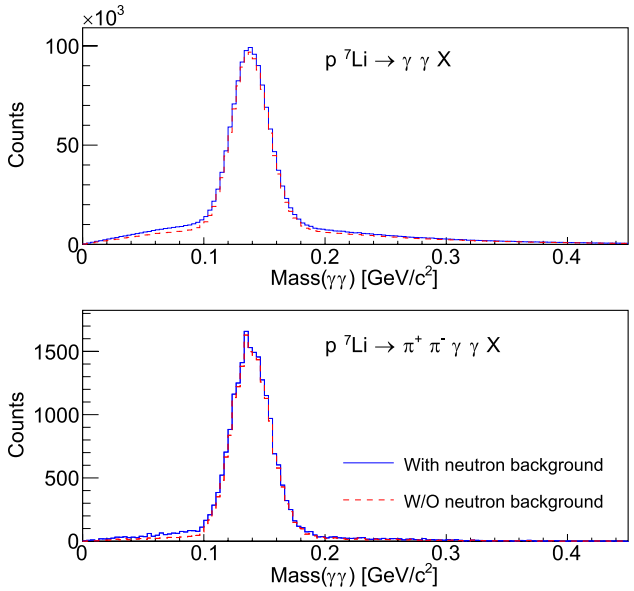

Fig. 3 (Color online) Invariant mass distributions of two γs from the simulations with and without the neutron contamination. The p-^{7}Li events are generated with the GiBUU package. The γs are detected under two different scenarios: (1) we assume that the calorimeter cannot distinguish the neutron from the photon (with neutron background) and (2) we assume that the calorimeter can well distinguish the neutron from the photon (without neutron background)

Additionally, due to the low light yield, the Cherenkov light being mainly in the UV range, and the detector being in a magnetic field, large-sized UV-sensitive SiPMs are required. These drawbacks present challenges for the use of lead glass in this project.

One option is to use the ADRIANO2 [125] dual-readout calorimeter currently being developed by the REDTOP group. This design combines scintillation materials and lead glass to capture both Cherenkov light and scintillation light signals. It employs longitudinal layering and a readout to provide excellent energy resolution and additional capability for low-energy particle identification. This design addresses the shortcomings of using lead glass only.

By applying a full-silicon tracker with small pixel size, the momenta of charged particles are precisely measured with a high event rate, and the sizes of all detectors scale down depending on the size of the inner tracker. This is a compact spectrometer with a large acceptance for fixed-target experiments and competitive functions. The LGAD detector for time-of-flight measurement has a low time resolution and extremely low material budget. The lead glass calorimeter is effective in reducing the neutron background, but its energy resolution is poor. We also look for new EM calorimeter technologies capable of working in a high event-rate environment. Therefore, using the current spectrometer design for the Huizhou η factory, we focus more on the charged decay channels of η mesons. The radiation dose

for the spectrometer was simulated using both Geant4 [118–120] and FLUKA [126–128]. Under the condition of a 100-MHz inelastic scattering rate, over a one-month data acquisition period, the inner-most LGAD is expected to experience a maximum 1 MeV neutron equivalent fluence of $3 \times 10^{12}\ n_{eq}/cm^2$ and a maximum dose of 200 Gy. Meanwhile, the lead glass of EM calorimeter is expected to experience a maximum 1 MeV neutron equivalent fluence of $5 \times 10^{11}\ n_{eq}/cm^2$ and maximum dose of 100 Gy. Thus, these subsystems can survive for several years before significant radiation damage occurs.

4 Preliminary results of simulations

To determine the physics impact and feasibility of the experiment, we performed simulations of some golden channels for the Huizhou η factory project. The simulation study is the first step for us to acquire the details regarding the resolutions, efficiency of the signal channel, background distribution, precision of the planed measurement, and/or sensitivity to new physics.

For the background events in *p–A* collisions, we used the GiBUU event generator [121–124] to perform the simulation. GiBUU is suitable for proton-induced nuclear reactions from low to intermediate energies, with final-state interactions being handled well [121]. The GiBUU event generator is based on the dynamic evolution of a colliding nucleus–nucleus system within the relativistic Boltzmann–Uehling–Uhlenbeck framework, which considers the hadronic potentials, equation of state of nuclear matter, and collision terms. In GiBUU, low-energy collision is dominated by resonance processes, while high-energy collision is described by a string fragmentation model implemented in Pythia. For η production, $N^*(1720)$ in the process $NN \rightarrow NR$ plays a dominant role [129]. Thus, the GiBUU event generator perfectly covers the kinematical regions of the HIAF and CiADS accelerator facilities.

In our simulation, the kinematic energy of the proton beam was 1.8 GeV, which is slightly below the ρ meson production threshold to lower the background. Using the lithium target, we found that the number of neutrons is approximately 1000 times the number of η mesons, and the number of π^0 mesons is approximately 50 times that of η mesons. We further coded the decay chains of π^0 and η. For signal event generation of dark portal particles, we constructed a simple event generator for the channels of interest. We also used another BUU generator [130] and the Urqmd package [131–133] to estimate the η production cross-section. The η production probability was 0.76% for inelastic collisions.

To quantify the detection efficiency and resolutions, we developed a detector simulation package ChnsRoot, which is based on the FairRoot framework [134, 135]. Currently, we have a reliable, fast simulation tool based on parameterizations validated by Geant4 simulations. The inner-most and outer-most radii of the silicon pixel tracker are 7.5 cm and 27.5 cm, respectively. The magnetic field strength is 0.8 Tesla. The energy resolution of the calorimeter is $\delta(E)/E = \sqrt{a^2 + b^2/(E/\mathrm{GeV})}$ for photons, with $a = 0.028$ and $b = 0.056$ estimated using Geant4. The neutron efficiency of the calorimeter as a function of energy and scattering angle was also studied in detail with Geant4. Calorimetric responses to different types of particles were carefully studied to achieve a realistic fast spectrometer simulation.

To understand the physics impact of the measurement, the statistics of the produced η samples was the most important input for the simulation. To be conservative in our experimental projections, in this simulation, we considered a prior experiment with only one month of operation. Based on the evaluated luminosity and p–*A* cross section, the potential production rate of η can exceed $10^8\ s^{-1}$, at an inelastic event rate of approximately $10^{10}\ s^{-1}$. A silicon pixel detector with a high granularity can operate at a high event rate (> 100 MHz) without a significant pile-up of events. However, considering the radiation hardness of the detector, and limits of the current data acquisition (DAQ) system, we make a notably conservative estimate of the event rate for the Huizhou η factory experiment. The event rate of inelastic scattering is assumed to be 100 MHz, and the η production rate is approximately 760 KHz. We also assumed a conservative duty factor for the accelerator of which is 30%. Using these settings, the number of η mesons produced is 5.9×10^{11} for the first experiment with only one month of running time. Thus, in the following simulations, we assume that only 5.9×10^{11} eta mesons were produced in the previous experiment.

The statistics of η meson samples can be increased to magnitudes higher, as the experiment will run for years. The event rate can also be increased with improvements in the detector radiation hardness and speed of DAQ system, and the proton beam can be delivered to the high-energy terminal with a high duty factor.

4.1 Dark photon search

The decay channel $\eta \rightarrow e^+e^-\gamma$ is particularly interesting because this channel is relevant to the search for the dark photon [34–37] and light protophobic X17 boson [5–7], which decay into an electron–positron pair. Simultaneously, from the precise measurement of this channel, we can precisely extract the transition form factor of η, which is an important input for the theoretical calculation of muon anomalous moment $(g-2)_\mu$. The dark photon is the most popular type of dark portal particle, and it feebly connects

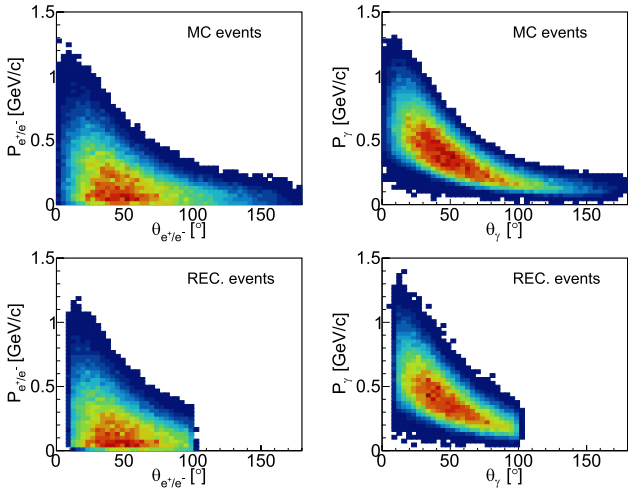

Fig. 4 (Color online) Momentum v.s. angle distributions of the final-state particles of $\eta \to e^+e^-\gamma$ decay channel. The top pads show the kinematic distributions of the final states from the event generator, while the bottom pads show the kinematic distributions of the reconstructed particles from the fast detector simulation. The designed spectrometer covers the main and large kinematic region of the final-state particles

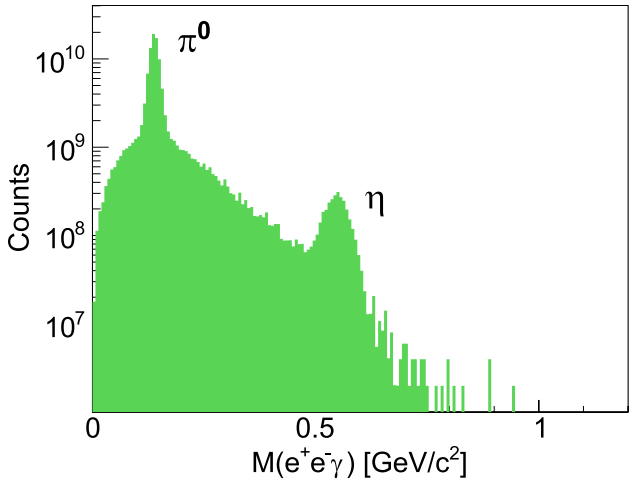

Fig. 5 (Color online) Invariant mass distribution of $e^+e^-\gamma$ from the simulation data for one-month running of Huizhou η factory experiment

the SM model sector with the possible hidden sector. Here, we focus on the physics impact on the dark photon from the simulation data of the Huizhou η factory experiment.

Figure 4 shows the kinematic distributions of the final-state particles of channel $e^+e^-\gamma$, from the event generator and particle reconstruction in the spectrometer simulation. Evidently, most of the final electrons have a low momentum (< 0.5 GeV/c) and go to angles from 10° to 100°. The average energy of the final photon is approximately 0.4 GeV, and the photons have similar electron-scattering angles. The designed spectrometer covers most of the electrons and photons, and the overall efficiency of the channel is estimated to be 60% using the simulation. Low-energy electrons can be identified effectively using energy decomposition dE/dx measured by a silicon pixel tracker. A high-energy electron can be identified using the calorimeter, as the pion initiates few Cherenkov photons in the lead glass calorimeter.

The distribution of the reconstructed invariant mass of $e^+e^-\gamma$ is shown in Fig. 5. Clearly, the peaks of π^0 and η have a low background underneath. Owing to suppression of the bremsstrahlung radiations in the proton-scattering process, the electron and photon backgrounds are not significant. η samples with a high purity can be selected by performing a cut on the invariant mass of $e^+e^-\gamma$. In this simulation, the invariant mass must be within the range of $[m_\eta - 3\sigma, m_\eta + 3\sigma]$.

To estimate the sensitivity of the proposed experiment to the dark photon, we carefully studied the background distribution through the simulation. The background events are generated using GiBUU with some decay chains added by us. In the simulation data, there is no bump in the invariant mass distribution of electrons and positions. We assume that there is no dark photon in the simulation and the invariant mass distribution of e^+e^- is the pure background distribution. No observation of the dark photon means that the statistical significance of the dark photon peak is less than 3σ. Consequently, we get a formula for the branching-ratio (BR) upper limit of the dark photon channel as follows:

$$\mathrm{BR}^{\mathrm{up}} = \frac{3 \times \sqrt{N_{\mathrm{bg}} \times \epsilon_{\mathrm{bg}}}}{N_\eta \times \epsilon_{\mathrm{sig}}}, \tag{1}$$

where N_{bg} is the number of background events, ϵ_{bg} is efficiency for the background event, N_η is the total number of eta mesons produced in the experiment, and ϵ_{sig} is the efficiency of the dark photon channel. $N_{\mathrm{bg}} \times \epsilon_{\mathrm{bg}}$ is actually the number of background events survived after all event selections. Based on the simulation of a one-month experiment of the Huizhou η factory, the BR upper limit of dark photon in η decay was evaluated and is shown in Fig. 6. The sensitivity of the kinematic mixing parameter ϵ^2 is closely related to the upper limit of the branching ratio, which is expressed as

$$S(\epsilon^2) = \frac{\mathrm{BR}^{\mathrm{up}}}{2|F(m_{\mathrm{A}}^2)|^2 \left(1 - \frac{m_{\mathrm{A}}^2}{m_\eta^2}\right)^3}, \tag{2}$$

where m_{A} and m_η are the masses of the dark photon and η meson, respectively, and F denotes the transition form factor of η. The final ϵ^2 sensitivity of the one-month experiment to the dark photon is shown in Fig. 7. Our simulation indicates significant sensitivity to ϵ^2 below 10^{-7}, which surpasses

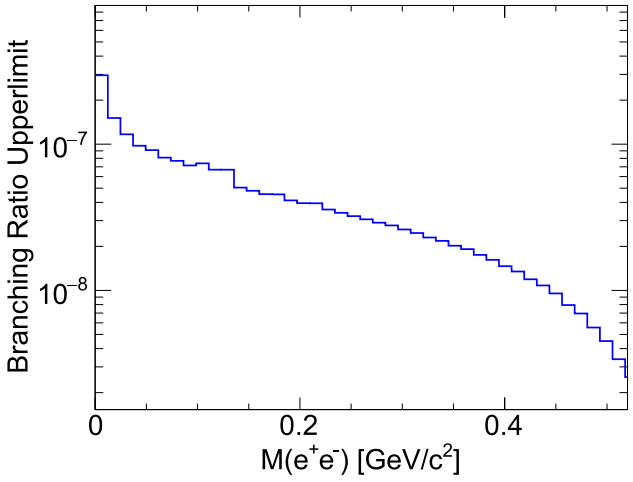

Fig. 6 (Color online) Estimated branching-ratio upper limit of dark photon for one-month running of Huizhou η factory experiment, under a conservative event rate of 100 MHz of inelastic reactions

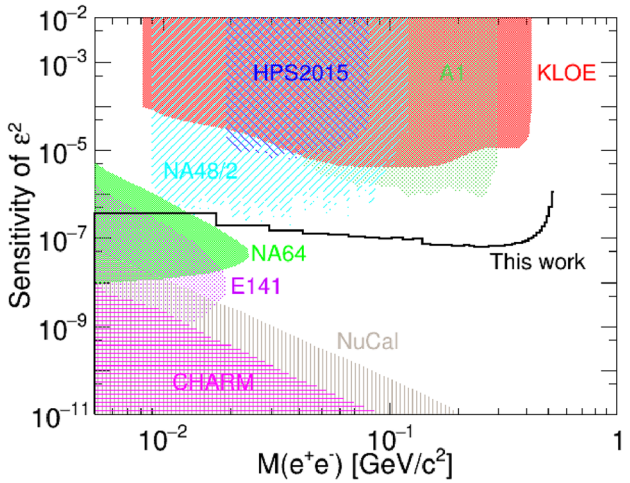

Fig. 7 (Color online) Estimated ε^2 sensitivity of dark photon for one-month running of Huizhou η factory experiment, under a conservative event rate of 100 MHz of inelastic reactions. The shaded exclusion areas in the figure corresponding to previous experiments (HPS2015, A1@MAMI, KLOE, NA48/2, NA64, E141, NuCal, and CHARM) are taken from Refs. [136–144]

the precision of previous experimental measurements (HPS2015 [136], A1@MAMI [137], KLOE [138], NA48/2 [139], NA64 [140], E141 [141], NuCal [142, 143], and CHARM [144]). The proposed experiment will be a valuable complement to other dark photon searches. After years of running of the experiment, the parameter space below the η mass will be almost ruled out when the results are considered in conjunction with the findings of many other experiments worldwide [136, 137, 142–150].

4.2 Light dark Higgs search

The light dark Higgs [38–44] is another representative dark portal particle, which couples the hidden scalar field with the Higgs doublet. Thus, the dark Higgs is weakly connected to leptons and quarks via the Yukawa coupling. Therefore, the dark Higgs can be produced in the hadronic process and can decay into lepton and quark pairs. In a hadrophilic scalar model, the dark Higgs mainly couples to the up quark; thus, it predominantly decays into pions. At the Huizhou ηfactory, we could search for the dark Higgs in the following channels: $\eta \to \pi^0 h \to \pi^0 e^+ e^-$ and $\eta \to \pi^0 h \to \pi^0 \pi^+ \pi^-$. In these η rare decay channels, a bump in the invariant mass distribution of e^+e^- or $\pi^+\pi^-$ is a clear signal of the possible dark scalar particle.

The distribution of reconstructed invariant mass of $\pi^+\pi^-\pi^0$ is shown in Fig. 8. The peak of η meson with a low background underneath is evident. In the GiBUU simulation, the background from the direct multi-pion production is low compared to the η production because the incident energy of the proton is low (1.8 GeV). η samples from $\pi^+\pi^-\pi^0$ can be selected with a high purity by performing a cut on the invariant mass of $\pi^+\pi^-\pi^0$ in the range of $[m_\eta - 3\sigma, m_\eta + 3\sigma]$. The low background does not hinder our explorations much for the rare decays of η meson.

From the simulation, the efficiencies of the $\pi^0 e^+ e^-$ and $\pi^0\pi^+\pi^-$ channels are all above 40% with the conceptual design of the spectrometer. The resolutions for the invariant masses of e^+e^- and $\pi^+\pi^-$ are 2 MeV/c^2 and 1 MeV/c^2, respectively. In this study, the bin width for the invariant mass was six times greater than the resolution. The background distributions without the dark Higgs particle are simulated using the GiBUU event generator, and the total

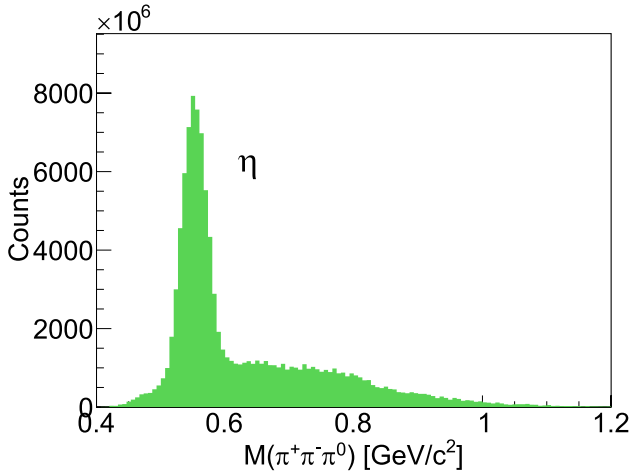

Fig. 8 (Color online) Invariant mass distribution of $\pi^+\pi^-\pi^0$ from the simulation data for one-month running of Huizhou η factory experiment

number of inelastic scattering events scales up to 5.9×10^{11}. Because there are no dark Higgs observed in our simulation data, the upper limit of the branching ratio of the dark Higgs particle is given by the formula in Eq. (1). The BR upper limits of the light dark Higgs particle in $\pi^0 e^+ e^-$ and $\pi^0\pi^+\pi^-$ channels are shown in Figs. 9 and 10, respectively, as a function of the mass of the dark Higgs.

As evident from Fig. 10, the BR upper limit of dark Higgs in the $\eta \to \pi^0\pi^+\pi^-$ channel lies between 10^{-6} and 10^{-7} for one-month running of the experiment. As shown in Fig. 9, the upper limit in the $\pi^0 e^+ e^-$ channel is below 10^{-8} in most ranges of the dark Higgs mass. This is mainly due to the lower electron background in $p - A$ collisions, compared to the strong pion background. Moreover, the upper limit in the e^+e^- channel decreases quickly, reaching a value below 10^{-8} when the mass exceeds 0.14 GeV. This is because most of the e^+e^- background originates from π^0 decay. Therefore, the e^+e^- channel offers the advantage of searching the dark Higgs with a higher mass than the pion. With years running of the Huizhou η factory experiment, we are confident that the accumulated data will provide strong constraints on the possible dark Higgs particle.

Under the hadrophilic scalar model [40, 41], the sensitivity to the parameter g_u (coupling of the dark scalar to the first-generation quark) is computed and shown in Fig. 11, compared with the constraints provided by previous experimental data (BESIII [151], KLOE [83], MAMI [152], CHARM [153, 154], and SN1987A [40]). The g_u sensitivity from one-month running of the proposed Huizhou η factory will exceed the current experimental limits in the accessed mass range. The proposed super η factory will play an important role in the search for light dark scalar portal particles.

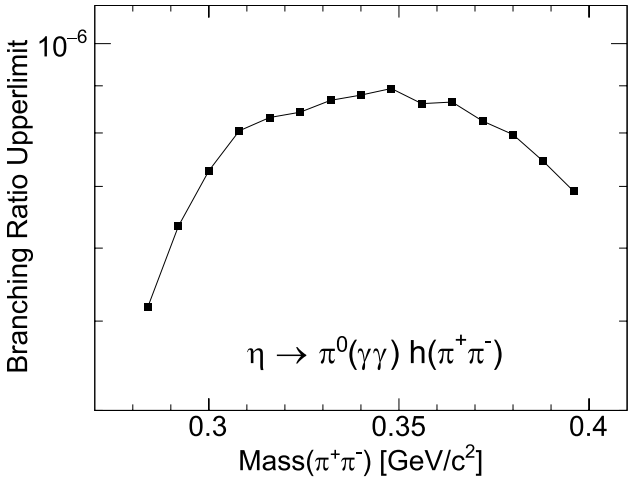

Fig. 10 (Color online) Estimated branching-ratio upper limit of light dark Higgs particle from $\pi^0\pi^+\pi^-$ channel for one-month running of Huizhou η factory experiment, under a conservative event rate of 100 MHz of inelastic reactions. The invariant mass of $\pi^0\pi^+\pi^-$ is required to be in the η mass region

4.3 C and CP violation in $\eta \to \pi^+\pi^-\pi^0$

The CP violation in the flavor-nondiagonal process owing to the Cabibbo–Kobayashi–Maskawa (CKM) matrix phase is insufficient to explain the matter–antimatter asymmetry in the universe. Therefore, the search for new sources and

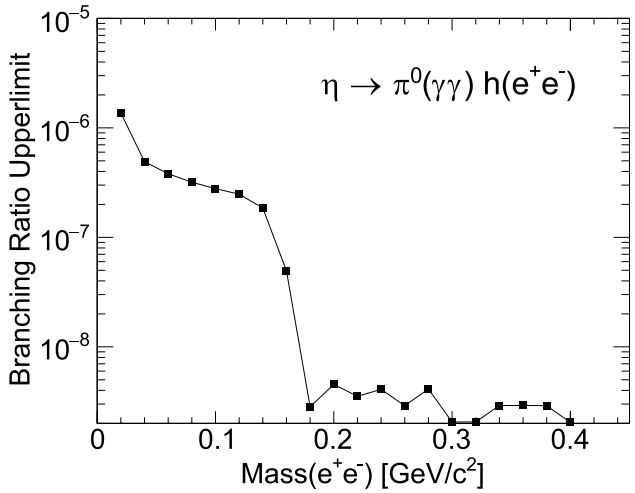

Fig. 9 (Color online) Estimated branching-ratio upper limit of light dark Higgs particle from $\pi^0 e^+ e^-$ channel for one-month running of Huizhou η factory experiment, under a conservative event rate of 100 MHz of inelastic reactions. The invariant mass of $\pi^0 e^+ e^-$ is required to be in the η mass region

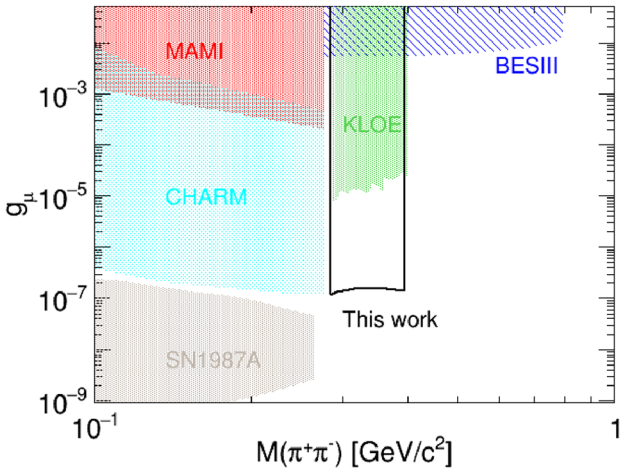

Fig. 11 (Color online) Estimated g_u sensitivity of light dark Higgs particle in a hadrophilic scalar model [40, 41], for one-month running of Huizhou η factory experiment, under a conservative event rate of 100 MHz of inelastic reactions. The previous experimental data for the shaded exclusion areas (BESIII, KLOE, MAMI, CHARM, and SN1987A) in the figure are taken from Refs. [40, 83, 151–154]

flavor-diagonal CP violation has become popular in the field of high-energy physics. The $\pi^+\pi^-\pi^0$ decay channel of the η meson is of particular interests, as it provides a unique process to probe the flavor-diagonal C and CP violation beyond the SM. This type of CP violation is not constrained by measurement of the nucleon electro-dipole moment (EDM). Thus, high-precision experimental studies have been lacking in this regard [33]. Because of the interference between the C-conserving and C-violating amplitudes, the CP violation signal can be large. Small C and CP violations can be detected from a precise measurement of the mirror symmetry in the Dalitz decay plot of the $\pi^+\pi^-\pi^0$ channel.

The direct observable of the charge asymmetry and CP violation is mirror symmetry breaking in the Dalitz plot of $\eta \to \pi^+\pi^-\pi^0$, that is, asymmetry under the exchange of u and t ($u \equiv (p_{\pi^+} + p_{\pi^0})^2$, $t \equiv (p_{\pi^-} + p_{\pi^0})^2$, and $s \equiv (p_{\pi^+} + p_{\pi^-})^2$). The C and CP violation is reflected in the asymmetry of the decay events of $u > t$ and $u < t$. Typically, mirror asymmetry is vividly illustrated in the Dalitz plot of X and Y variables, which are defined as:

$$\begin{aligned} X &\equiv \sqrt{3}\frac{T_{\pi^+} - T_{\pi^-}}{Q_\eta} = \frac{\sqrt{3}}{2m_\eta Q_\eta}(u - t), \\ Y &\equiv \frac{3T_{\pi^0}}{Q_\eta} - 1 = \frac{3}{2m_\eta Q_\eta}[(m_\eta - m_{\pi^0})^2 - s] - 1, \end{aligned} \tag{3}$$

where $Q_\eta = m_\eta - m_{\pi^+} - m_{\pi^-} - m_{\pi^0}$ and T_{π^i} are the total kinematic energy and kinematic energy of π^i in the η rest frame, respectively. The distribution asymmetry across $X = 0$ is an observable of the new type of CP violation. The Dalitz distribution of the decay probability can be conveniently parameterized as a polynomial expansion expressed as

$$\begin{aligned} N(X, Y) = N_0(1 + aY + bY^2 + cX + dX^2 + eXY \\ + fY^3 + gX^2Y + hXY^2 + lX^3 + ...), \end{aligned} \tag{4}$$

where a, b, c... are free parameters. The nonzero values of the parameters c, e, h, or l are a strong indication for the flavor-diagonal C and CP violation.

The $\pi^+\pi^-\pi^0$ channel is a major decay channel of the η meson, and we can obtain a huge number of decay events from the Huizhou η factory experiment. From the simulation, the efficiency for the 3 pion channel is estimated to be approximately 45%. The event distributions in the different X and Y bins are shown in Fig. 12 for one-month running of the experiment. The statistical error bars are too small to display in the figure. We performed a model fit to the data using Eq. (4). The uncertainty of the parameter c is approximately 5×10^{-5}, which is two orders of magnitude smaller than those of the current analyses of COSY and KLOE-II data [77, 83]. Over the years running the project, the C and CP violation can be tested at a satisfactory level of precision.

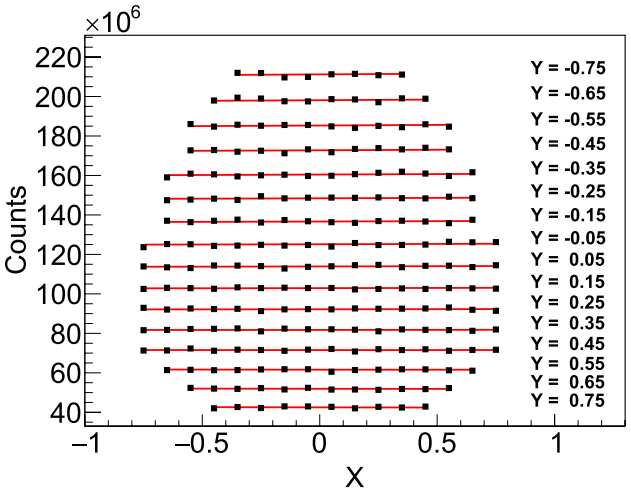

Fig. 12 (Color online) Event distributions of $\eta \to \pi^+\pi^-\pi^0$ decay channel (black squares) in different X and Y bins for one-month running of Huizhou η factory experiment, under a conservative event rate of 100 MHz of inelastic reactions. The Dalitz distribution of $\eta \to \pi^+\pi^-\pi^0$ is fitted with a simple model (red lines). See the main text for more explanations

4.4 Low-background η data from exclusive channel pd $\to \eta$ ^{3}He

Here, we emphasize that low-background data of η mesons can be obtained at the Huizhou η factory via the ^{3}He tagged events of the reaction pd $\to \eta$ ^{3}He. In addition to the exclusivity of the measurement, the momentum and angle of the final-state particle are highly correlated in the two-body-to-two-body scattering process. By tagging ^{3}He and cutting the momentum-angle correlation, the background is significantly reduced. The cross-section of the pd $\to \eta$ ^{3}He reaction is not small [101, 155–159]; it is 0.4 μb and near the production threshold measured by the COSY-ANKE collaboration [157]. The multiplicity of the final particles using deuterium target is much smaller than that using other nuclear targets. Therefore, the event rate for pd $\to \eta$ ^{3}He measurement can be set at a much higher rate to increase the amount of low-background data.

Figure 13 shows the two-dimensional kinematic distributions of ^{3}He and η in the momentum vs. angle plane. Evidently, the final ^{3}He mainly goes to the region of scattering angle from 15° to 25°, whereas the η meson has a scattering angle mainly in the range from 20° to 70°. The conceptual design of the spectrometer is suitable for tagging ^{3}He and collecting the decay particles of the η meson with high acceptance. As evident from Fig. 13, the momentum

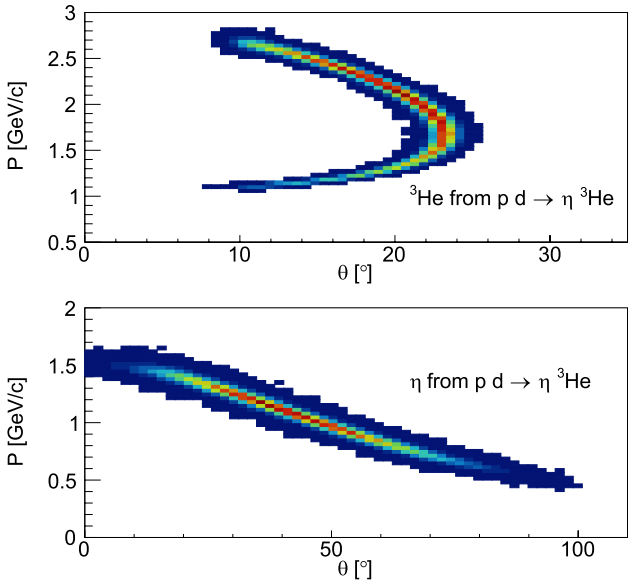

Fig. 13 (Color online) Kinematic distributions of the reconstructed ^{3}He and η from a fast simulation of the spectrometer. The scattering angle and momentum are highly correlated for the particles in the reaction pd $\rightarrow \eta\, ^3$He. The angular and momentum resolutions are small from the silicon pixel tracker

and angular resolutions of the silicon pixel tracker are excellent for selecting exclusive events of pd $\rightarrow \eta\, ^3$He.

In short, using the high-intensity proton beam and deuterium target, we can measure with both high luminosity and precision at the Huizhou η factory. These high-statistic and low-background data are valuable in the search for new light particles, looking for the violations of CP and other discrete symmetries, measuring the transition form factor and $u - d$ quark mass difference, and testing the low-energy effective theory of the strong interaction. The systematic uncertainty from the background can be well controlled with the tagged η data of pd $\rightarrow \eta\, ^3$He.

5 Summary and outlook

A super η factory at Huizhou is proposed for pursuing a variety of meaningful and challenging physical goals. HIAF accelerator complex and conceptual design of the spectrometer are briefly discussed. More than 10^{13} η mesons can be produced with 100% duty factor of the accelerator. The performance of the spectrometer is studied with Geant4 simulation, demonstrating satisfactory efficiency and resolution. The designed spectrometer is particularly useful for the detection of charged particles and exhibits the radiation hardness required for high-luminosity experiments.

Through simulations, some key channels of the Huizhou η factory experiment are investigated. The preliminary results from the fast simulation show that the Huizhou η factory will play a crucial role in searching for the predicted light dark portal particles and new sources of CP violation. The proposed experiment has the potential to significantly constrain the parameter space of the dark photon in the low-mass region together with other experiments. The sensitivity to light dark scalar particle is estimated to be at an unprecedented level. The C and CP violation in the channel $\eta \rightarrow \pi^+\pi^-\pi^0$ can be measured at least two orders of magnitude more precisely than up-to-date measurements worldwide. Based on the simulation, the conceptual design of the spectrometer is capable of measuring the tagged η events of the reaction pd $\rightarrow \eta\, ^3$He. The tagging ^{3}He method provides a measurement of both high statistics and low background, which is vital for the precise study of η physics.

After completing the planned accumulation of η decay samples, we could increase the beam energy and produce the η' meson. The physical goals of high-precision studies of η' meson decay closely resemble those of the η meson. An advantage of studying η' decay is the ability to explore dark portal particles over a wider mass range, given that the η' meson is heavier than the η meson. High-precision studies could also be conducted using the same spectrometer on η' and ϕ meson decays, thereby boosting the discovery potential of the proposed Huizhou η factory project.

To further improve the discovery potential of the spectrometer, it is essential to enhance its capacity to detect neutral particles. The current lead glass EM calorimeter exhibits standard energy resolution; therefore, new calorimeter technologies with fast response times (< 100 ps) and low energy resolution (< 3.5% at 1 GeV) is imperative. With the rapid development of silicon photomultipliers and electronics, dual-readout calorimetry for collecting scintillation and Cherenkov photons is a viable option for updating the EM calorimeter. The scintillation material significantly improves the energy resolution, while the Cherenkov light provides a sharp time resolution. The particle identification ability can also be enhanced using the dual-readout calorimeter by comparing scintillation and Cherenkov signal amplitudes. Future developments in silicon pixel detectors and electronics will benefit the proposed Huizhou η factory project, enabling improvements in radiation hardness and resolutions, which increase the event-rate limit for the planned high-luminosity experiments.

Author contributions All authors contributed to the study conception and design. Material preparation, Monte-Carlo simulation and analysis were performed by Xiong-Hong He, Yang Liu, Ye Tian and Rong Wang. The first draft of the manuscript was written by Rong Wang, and all authors commented on previous versions of the manuscript. All authors read and approved the final manuscript.

Data availability The data that support the findings of this study are openly available in Science Data Bank at https://cstr.cn/31253.11.scien

cedb.j00186.00623 and https://doi.org/10.57760/sciencedb.j00186.00623.

Declarations

Conflict of interest Cheng-Xin Zhao is an editorial board member for Nuclear Science and Techniques and was not involved in the editorial review, or the decision to publish this article. All authors declare that there are no conflict of interest.

References

1. *Fundamental Physics at the Intensity Frontier*. arXiv:1205.2671, https://doi.org/10.2172/1042577
2. D.P. Aguillard, T. Albahri, D. Allspach et al., Measurement of the positive muon anomalous magnetic moment to 0.20 ppm. Phys. Rev. Lett. **131**, 161802 (2023). https://doi.org/10.1103/PhysRevLett.131.161802. arXiv:2308.06230
3. B. Abi, T. Albahri, S. Al-Kilani et al., Measurement of the positive muon anomalous magnetic moment to 0.46 ppm. Phys. Rev. Lett. **126**, 141801 (2021). https://doi.org/10.1103/PhysRevLett.126.141801. arXiv:2104.03281
4. T. Albahri, A. Anastasi, A. Anisenkov et al., Measurement of the anomalous precession frequency of the muon in the fermilab muon $g-2$ experiment. Phys. Rev. D **103**, 072002 (2021). https://doi.org/10.1103/PhysRevD.103.072002. arXiv:2104.03247
5. A.J. Krasznahorkay, M. Csatlós, L. Csige et al., Observation of anomalous internal pair creation in ^{8}Be: A possible indication of a light, neutral boson. Phys. Rev. Lett. **116**, 042501 (2016). https://doi.org/10.1103/PhysRevLett.116.042501. arXiv:1504.01527
6. J.L. Feng, B. Fornal, I. Galon et al., Protophobic fifth-force interpretation of the observed anomaly in ^{8}Be nuclear transitions. Phys. Rev. Lett. **117**, 071803 (2016). https://doi.org/10.1103/PhysRevLett.117.071803. arXiv:1604.07411
7. J.L. Feng, B. Fornal, I. Galon et al., Particle physics models for the 17 MeV anomaly in beryllium nuclear decays. Phys. Rev. D **95**, 035017 (2017). https://doi.org/10.1103/PhysRevD.95.035017. arXiv:1608.03591
8. LHCb collaboration, Addendum: Test of lepton universality in beauty-quark decays. Nature Phys. **19**, 1517 (2023). https://doi.org/10.1038/s41567-023-02095-3
9. R. Aaij, A.S.W. Abdelmotteleb, C. Abellán Beteta et al., Tests of lepton universality using $B^0 \to K^0_S \ell^+ \ell^-$ and $B^+ \to K^{*+} \ell^+ \ell^-$ decays. Phys. Rev. Lett. **128**, 191802 (2022). https://doi.org/10.1103/PhysRevLett.128.191802. arXiv:2110.09501
10. R. Aaij, C. Abellán Beteta, T. Ackernley et al., Test of lepton universality with $\Lambda^0_b \to pK^-\ell^+\ell^-$ decays. J. High Energ. Phys. **2020**, 40 (2020). https://doi.org/10.1007/JHEP05(2020)040. arXiv:1912.08139,
11. R. Alonso, B. Grinstein, J. Martin Camalich, Lepton universality violation and lepton flavor conservation in B-meson decays. JHEP **10**, 184 (2015). https://doi.org/10.1007/JHEP10(2015)184. arXiv:1505.05164
12. S. Patnaik, L. Nayak, R. Singh, Assessing lepton flavor universality violations in semileptonic decays. arXiv:2308.05677
13. G. Ambrosi et al., Direct detection of a break in the teraelectronvolt cosmic-ray spectrum of electrons and positrons. Nature **552**, 63–66 (2017). https://doi.org/10.1038/nature24475. arXiv:1711.10981
14. O. Adriani, G.C. Barbarino, G.A. Bazilevskaya et al., An anomalous positron abundance in cosmic rays with energies 1.5–100 GeV. Nature **458**, 607–609 (2009). https://doi.org/10.1038/nature07942. arXiv:0810.4995
15. J. Chang, J.H. Adams, H.S. Ahn et al., An excess of cosmic ray electrons at energies of 300–800 GeV. Nature **456**, 362–365 (2008). https://doi.org/10.1038/nature07477
16. F. Aharonian, A.G. Akhperjanian, U. Barres de Almeida et al., The energy spectrum of cosmic-ray electrons at TeV energies. Phys. Rev. Lett. **101**, 261104 (2008). https://doi.org/10.1103/PhysRevLett.101.261104. arXiv:0811.3894
17. P. Jean, J. Knödlseder, V. Lonjou et al., Early SPI / INTEGRAL measurements of 511 keV line emission from the 4th quadrant of the Galaxy. Astron. Astrophys. **407**, L55 (2003). https://doi.org/10.1051/0004-6361:20031056. arXiv:astro-ph/0309484
18. A. Arbey, F. Mahmoudi, Dark matter and the early Universe: A review. Prog. Part. Nucl. Phys. **119**, 103865 (2021). https://doi.org/10.1016/j.ppnp.2021.103865. arXiv:2104.11488
19. E. Oks, Brief review of recent advances in understanding aip conf proc and dark energy. New Astron. Rev. **93**, 101632 (2021). https://doi.org/10.1016/j.newar.2021.101632. arXiv:2111.00363
20. G. Bertone, T.M.P. Tait, A new era in the search for aip conf proc. Nature **562**, 51–56 (2018). https://doi.org/10.1038/s41586-018-0542-z
21. B.L. Young, A survey of aip conf proc and related topics in cosmology. Front. Phys. (Beijing) **12**, 121201 (2017). https://doi.org/10.1007/s11467-016-0583-4
22. J.L. Feng, Dark matter candidates from particle physics and methods of detection. Ann. Rev. Astron. Astrophys. **48**, 495–545 (2010). https://doi.org/10.1146/annurev-astro-082708-101659. arXiv:1003.0904
23. J. Frieman, M. Turner, D. Huterer, Dark energy and the accelerating universe. Ann. Rev. Astron. Astrophys. **46**, 385–432 (2008). https://doi.org/10.1146/annurev.astro.46.060407.145243. arXiv:0803.0982
24. S. Vagnozzi, L. Visinelli, P. Brax et al., Direct detection of dark energy: The xenon1t excess and future prospects. Phys. Rev. D **104**, 063023 (2021). https://doi.org/10.1103/PhysRevD.104.063023. arXiv:2103.15834
25. A. Joyce, L. Lombriser, F. Schmidt, Dark energy versus modified gravity. Ann. Rev. Nucl. Part. Sci. **66**, 95–122 (2016). https://doi.org/10.1146/annurev-nucl-102115-044553. arXiv:1601.06133
26. M. Li, X.D. Li, S. Wang et al., Dark energy: A brief review. Front. Phys. (Beijing) **8**, 828–846 (2013). https://doi.org/10.1007/s11467-013-0300-5
27. K. Arun, S.B. Gudennavar, C. Sivaram, Aip conf proc, dark energy, and alternate models: A review. Adv. Space Res. **60**, 166–186 (2017). https://doi.org/10.1016/j.asr.2017.03.043. arXiv:1704.06155
28. B. Batell, M. Pospelov, A. Ritz, Exploring portals to a hidden sector through fixed targets. Phys. Rev. D **80**, 095024 (2009). https://doi.org/10.1103/PhysRevD.80.095024. arXiv:0906.5614
29. G. Lanfranchi, M. Pospelov, P. Schuster, The search for feebly interacting particles. Ann. Rev. Nucl. Part. Sci. **71**, 279–313 (2021). https://doi.org/10.1146/annurev-nucl-102419-055056. arXiv:2011.02157
30. R.L. Workman, V.D. Burkert, V. Crede et al., Review of particle physics. PTEP **2022**, 083C01 (2022). https://doi.org/10.1093/ptep/ptac097
31. J. Elam et al., The REDTOP experiment: Rare η/η' Decays To Probe New Physics. arXiv:2203.07651
32. L. Gan, B. Kubis, E. Passemar et al., Precision tests of fundamental physics with η and η' mesons. Phys. Rept. **945**, 1–105 (2022). https://doi.org/10.1016/j.physrep.2021.11.001. arXiv:2007.00664

33. S. Gardner, J. Shi, Patterns of CP violation from mirror symmetry breaking in the $\eta \to \pi^+\pi^-\pi^0$ Dalitz plot. Phys. Rev. D **101**, 115038 (2020). https://doi.org/10.1103/PhysRevD.101.115038. arXiv:1903.11617
34. B. Holdom, Two U(1)'s and epsilon charge shifts. Phys. Lett. B **166**, 196–198 (1986). https://doi.org/10.1016/0370-2693(86)91377-8
35. P. Galison, A. Manohar, Two Z's or not two Z's? Phys. Lett. B **136**, 279–283 (1984). https://doi.org/10.1016/0370-2693(84)91161-4
36. P. Fayet, Extra U(1)'s and new forces. Nucl. Phys. B **347**, 743–768 (1990). https://doi.org/10.1016/0550-3213(90)90381-M
37. P. Fayet, On the search for a new spin 1 boson. Nucl. Phys. B **187**, 184–204 (1981). https://doi.org/10.1016/0550-3213(81)90122-X
38. C.P. Burgess, M. Pospelov, T. ter Veldhuis, The Minimal Model of nonbaryonic dark matter: A singlet scalar. Nucl. Phys. B **619**, 709–728 (2001). https://doi.org/10.1016/S0550-3213(01)00513-2. arXiv:hep-ph/0011335
39. D. O'Connell, M.J. Ramsey-Musolf, M.B. Wise, Minimal extension of the standard model scalar sector. Phys. Rev. D **75**, 037701 (2007). https://doi.org/10.1103/PhysRevD.75.037701. arXiv:hep-ph/0611014
40. B. Batell, A. Freitas, A. Ismail et al., Probing light aip conf proc with a hadrophilic scalar mediator. Phys. Rev. D **100**, 095020 (2019). https://doi.org/10.1103/PhysRevD.100.095020. arXiv:1812.05103
41. B. Batell, A. Freitas, A. Ismail et al., Flavor-specific scalar mediators. Phys. Rev. D **98**, 055026 (2018). https://doi.org/10.1103/PhysRevD.98.055026. arXiv:1712.10022
42. B. Patt, F. Wilczek, Higgs-field portal into hidden sectors. arXiv:hep-ph/0605188
43. V. Silveira, A. Zee, Scalar phantoms. Phys. Lett. B **161**, 136–140 (1985). https://doi.org/10.1016/0370-2693(85)90624-0
44. M. Pospelov, A. Ritz, M.B. Voloshin, Secluded wimp aip conf proc. Phys. Lett. B **662**, 53–61 (2008). https://doi.org/10.1016/j.physletb.2008.02.052. arXiv:0711.4866
45. H. Georgi, D.B. Kaplan, L. Randall, Manifesting the invisible axion at low-energies. Phys. Lett. B **169**, 73–78 (1986). https://doi.org/10.1016/0370-2693(86)90688-X
46. M. Bauer, M. Neubert, A. Thamm, Collider probes of axion-like particles. JHEP **12**, 044 (2017). https://doi.org/10.1007/JHEP12(2017)044. arXiv:1708.00443,
47. D. Aloni, Y. Soreq, M. Williams, Coupling qcd-scale axionlike particles to gluons. Phys. Rev. Lett. **123**, 031803 (2019). https://doi.org/10.1103/PhysRevLett.123.031803. arXiv:1811.03474
48. G. Landini, E. Meggiolaro, Study of the interactions of the axion with mesons and photons using a chiral effective lagrangian model. Eur. Phys. J. C **80**, 302 (2020). https://doi.org/10.1140/epjc/s10052-020-7849-2. arXiv:1906.03104
49. F. Ertas, F. Kahlhoefer, On the interplay between astrophysical and laboratory probes of MeV-scale axion-like particles. JHEP **07**, 050 (2020). https://doi.org/10.1007/JHEP07(2020)050. arXiv:2004.01193
50. D. Gorbunov, M. Shaposhnikov, How to find neutral leptons of the νmsm? JHEP **10**, 015 (2007). https://doi.org/10.1088/1126-6708/2007/10/015
51. A. Atre, T. Han, S. Pascoli et al., The search for heavy majorana neutrinos. JHEP **05**, 030 (2009). https://doi.org/10.1088/1126-6708/2009/05/030. arXiv:0901.3589
52. S.N. Gninenko, The miniboone anomaly and heavy neutrino decay. Phys. Rev. Lett. **103**, 241802 (2009). https://doi.org/10.1103/PhysRevLett.103.241802. arXiv:0902.3802
53. S. Weinberg, Phenomenological lagrangians. Physica A **96**, 327–340 (1979). https://doi.org/10.1016/0378-4371(79)90223-1
54. J. Gasser, H. Leutwyler, Chiral perturbation theory to one loop. Annals Phys. **158**, 142 (1984). https://doi.org/10.1016/0003-4916(84)90242-2
55. J. Gasser, H. Leutwyler, Chiral perturbation theory: Expansions in the mass of the strange quark. Nucl. Phys. B **250**, 465–516 (1985). https://doi.org/10.1016/0550-3213(85)90492-4
56. G. Ecker, Chiral perturbation theory. Prog. Part. Nucl. Phys. **35**, 1–80 (1995). https://doi.org/10.1016/0146-6410(95)00041-G. arXiv:hep-ph/9501357
57. A. Pich, Chiral perturbation theory. Rept. Prog. Phys. **58**, 563–610 (1995). https://doi.org/10.1088/0034-4885/58/6/001. arXiv:hep-ph/9502366
58. V. Bernard, U.G. Meissner, Chiral perturbation theory. Ann. Rev. Nucl. Part. Sci. **57**, 33–60 (2007). https://doi.org/10.1146/annurev.nucl.56.080805.140449. arXiv:hep-ph/0611231
59. P. Aguar-Bartolome, J.R.M. Annand, H.J. Arends et al., New determination of the η transition form factor in the Dalitz decay $\eta \to e^+e^-\gamma$ with the Crystal Ball/Taps detectors at the Mainz Microtron. Phys. Rev. C **89**, 044608 (2014). https://doi.org/10.1103/PhysRevC.89.044608. arXiv:1309.5648
60. P. Adlarson, F. Afzal, P. Aguar-Bartolomé et al., Measurement of the $\omega \to \pi^0 e^+e^-$ and $\eta \to e^+e^-\gamma$ Dalitz decays with the A2 setup at the Mainz Microtron. Phys. Rev. C **95**, 035208 (2017). https://doi.org/10.1103/PhysRevC.95.035208. arXiv:1609.04503
61. D. Pszczel, J. Stepaniak, Dielectron pairs from η meson decays at wasa detector. EPJ Web Conf. **199**, 02011 (2019). https://doi.org/10.1051/epjconf/201919902011
62. F. Ambrosino, A. Antonelli, M. Antonelli et al., Observation of the rare $\eta \to e^+e^-e^+e^-$ decay with the kloe experiment. Phys. Lett. B **702**, 324–328 (2011). https://doi.org/10.1016/j.physletb.2011.07.033. arXiv:1105.6067
63. M. Berlowski, Chr. Bargholtz, M. Bashkanov et al., Measurement of η meson decays into lepton-antilepton pairs. Phys. Rev. D **77**, 032004 (2008). https://doi.org/10.1103/PhysRevD.77.032004. arXiv:0711.3531
64. M. Ablikim, M.N. Achasov, X.C. Ai et al., Observation of the dalitz decay $\eta' \to \gamma e^+e^-$. Phys. Rev. D **92**, 012001 (2015). https://doi.org/10.1103/PhysRevD.92.012001. arXiv:1504.06016
65. R. Escribano, P. Masjuan, P. Sanchez-Puertas, The η transition form factor from space- and time-like experimental data. Eur. Phys. J. C **75**, 414 (2015). https://doi.org/10.1140/epjc/s10052-015-3642-z. arXiv:1504.07742
66. M. Gell-Mann, R.J. Oakes, B. Renner, Behavior of current divergences under $Su_3 \times Su_3$. Phys. Rev. **175**, 2195–2199 (1968). https://doi.org/10.1103/PhysRev.175.2195
67. S. Weinberg, The problem of mass. Trans. New York Acad. Sci. **38**, 185–201 (1977). https://doi.org/10.1111/j.2164-0947.1977.tb02958.x
68. R.F. Dashen, Chiral Su(3) $\otimes$ Su(3) as a symmetry of the strong interactions. Phys. Rev. **183**, 1245–1260 (1969). https://doi.org/10.1103/PhysRev.183.1245
69. J. Gasser, H. Leutwyler, eta$\to$3π to One Loop. Nucl. Phys. B **250**, 539–560 (1985). https://doi.org/10.1016/0550-3213(85)90494-8
70. D.B. Kaplan, A.V. Manohar, Current mass ratios of the light quarks. Phys. Rev. Lett. **56**, 2004 (1986). https://doi.org/10.1103/PhysRevLett.56.2004
71. H. Leutwyler, The ratios of the light quark masses. Phys. Lett. B **378**, 313–318 (1996). https://doi.org/10.1016/0370-2693(96)00386-3. arXiv:hep-ph/9602366
72. J. Wess, B. Zumino, Consequences of anomalous ward identities. Phys. Lett. B **37**, 95–97 (1971). https://doi.org/10.1016/0370-2693(71)90582-X
73. E. Witten, Global aspects of current algebra. Nucl. Phys. B **223**, 422–432 (1983). https://doi.org/10.1016/0550-3213(83)90063-9

74. A.M. Bernstein, B.R. Holstein, Neutral pion lifetime measurements and the qcd chiral anomaly. Rev. Mod. Phys. **85**, 49 (2013). https://doi.org/10.1103/RevModPhys.85.49. arXiv:1112.4809
75. M. Jetter, η→ $\pi^0\gamma\gamma$ to O(p^6) in chiral perturbation theory. Nucl. Phys. B **459**, 283–310 (1996). https://doi.org/10.1016/0550-3213(95)00598-6. arXiv:hep-ph/9508407
76. P. Adlarson, W. Augustyniak, W. Bardan et al., Search for c violation in the decay $\eta \to \pi^0 + e^+ + e^-$ with wasa-at-cosy. Phys. Lett. B **784**, 378–384 (2018). https://doi.org/10.1016/j.physletb.2018.07.017. arXiv:1802.08642
77. P. Adlarson, W. Augustyniak, W. Bardan et al., Measurement of the $\eta \to \pi^+\pi^-\pi^0$ dalitz plot distribution. Phys. Rev. C **90**, 045207 (2014). https://doi.org/10.1103/PhysRevC.90.045207. arXiv:1406.2505
78. N. Hüsken, K. Demmich, A. Khoukaz, η meson physics with wasa-at-cosy. EPJ Web Conf. **199**, 01006 (2019). https://doi.org/10.1051/epjconf/201919901006
79. R. Aaij, A.S.W. Abdelmotteleb, C. Abellan Beteta et al., Production of η and η' mesons in pp and pPb collisions. Phys. Rev. C **109**, 024907 (2024). https://doi.org/10.1103/PhysRevC.109.024907. arXiv:2310.17326
80. R. Aaij, B. Adeva, M. Adinolfi et al., Search for the cp-violating strong decays $\eta \to \pi^+\pi^-$ and $\eta'(958) \to \pi^+\pi^-$. Phys. Lett. B **764**, 233–240 (2017). https://doi.org/10.1016/j.physletb.2016.11.032. arXiv:1610.03666
81. W. Krzemien, E. Pérez del Rio, The KLOE-2 experiment: Overview of recent results. Int. J. Mod. Phys. A **34**, 1930012 (2019). https://doi.org/10.1142/S0217751X19300126. arXiv:1909.01233
82. D. Babusci, M. Berlowski, C. Bloise et al., Upper limit on the $\eta \to \pi^+\pi^-$ branching fraction with the KLOE experiment. J. High Energ. Phys. **2020**, 47 (2020). https://doi.org/10.1007/JHEP10(2020)047. arXiv:2006.14710
83. A. Anastasi, D. Babusci, G. Bencivenni et al., Precision measurement of the $\eta \to \pi^+\pi^-\pi^0$ dalitz plot distribution with the kloe detector. J. High Energ. Phys. **2016**, 19 (2016). https://doi.org/10.1007/JHEP05(2016)019. arXiv:1601.06985
84. F. Ambrosino, A. Antonelli, M. Antonelli et al., Measurement of the branching ratio and search for a cp violating asymmetry in the $\eta \to \pi^+\pi^-e^+e^-(\gamma)$ decay at kloe. Phys. Lett. B **675**, 283–288 (2009). https://doi.org/10.1016/j.physletb.2009.04.013. arXiv:0812.4830
85. M. Ablikim, M. N. Achasov, P. Adlarson et al., Measurement of the absolute branching fractions of $J/\psi \to \gamma\eta$ and η decay modes. Phys. Rev. D **104**, 092004 (2021). https://doi.org/10.1103/PhysRevD.104.092004. arXiv:2109.12812
86. M. Ablikim, M.N. Achasov, X.C. Ai et al., Measurement of the matrix elements for the decays $\eta \to \pi^+\pi^-\pi^0$ and $\eta/\eta' \to \pi^0\pi^0\pi^0$. Phys. Rev. D **92**, 012014 (2015). https://doi.org/10.1103/PhysRevD.92.012014. arXiv:1506.05360
87. M. Ablikim, M.N. Achasov, P. Adlarson et al., Evidence for the cusp effect in η' decays into $\eta\pi 0\pi 0$. Phys. Rev. Lett. **130**, 081901 (2023). https://doi.org/10. 1103/PhysRevLett.130.081901. arXiv:2207.01004
88. M. Ablikim, M. N. Achasov, S. Ahmed et al., Precision measurement of the branching fractions of η' decays. Phys. Rev. Lett. **122**, 142002 (2019). https://doi.org/10.1103/PhysRevLett.122.142002. arXiv:1902.03823
89. M. Ablikim, M. N. Achasov, S. Ahmed et al., Precision study of $\eta' \to \gamma\pi^+\pi^-$ decay dynamics. Phys. Rev. Lett. **120**, 242003 (2018). https://doi.org/10.1103/PhysRevLett.120.242003. arXiv:1712.01525
90. V.L. Kashevarov, P. Ott, S. Prakhov et al., Study of η and η' Photoproduction at MAMI. Phys. Rev. Lett. **118**, 212001 (2017). https://doi.org/10.1103/PhysRevLett.118.212001. arXiv:1701.04809
91. E.F. McNicoll, S. Prakhov, I.I. Strakovsky et al., Study of the $\gamma p- > \eta p$ reaction with the Crystal Ball detector at the Mainz Microtron (MAMI-C). Phys. Rev. C **82**, 035208 (2010). https://doi.org/10.1103/PhysRevC.82.035208
92. L. Gan et al., Update to the JEF proposal (pr12-14-004)., https://www.jlab.org/exp_prog/proposals/17/C12-14-004.pdf, accessed June 18, 2024
93. H. Primakoff, Photoproduction of neutral mesons in nuclear electric fields and the mean life of the neutral meson. Phys. Rev. **81**, 899 (1951). https://doi.org/10.1103/PhysRev.81.899
94. I. Larin, D. McNulty, E. Clinton et al., A new measurement of the π^0 radiative decay width. Phys. Rev. Lett. **106**, 162303 (2011). https://doi.org/10.1103/PhysRevLett.106.162303. arXiv:1009.1681
95. I. Larin, Y. Zhang, A. Gasparian et al., Precision measurement of the neutral pion lifetime. Science **368**, 506–509 (2020). https://doi.org/10.1126/science.aay6641
96. S. Adhikari, C.S. Akondi, H. Al Ghoul et al., The GLUEX beamline and detector. Nucl. Instrum. Meth. A **987**, 164807 (2021). https://doi.org/10.1016/j.nima.2020.164807. arXiv:2005.14272
97. A. Asaturyan, F. Barbosa, V. Berdnikov et al., Electromagnetic calorimeters based on scintillating lead tungstate crystals for experiments at jefferson lab. Nucl. Instrum. Meth. A **1013**, 165683 (2021). https://doi.org/10.1016/j.nima.2021.165683
98. J.C. Yang, J.W. Xia, G.Q. Xiao et al., High intensity heavy ion accelerator facility (hiaf) in china. Nucl. Instrum. Meth. B **317**, 263–265 (2013). https://doi.org/10.1016/j.nimb.2013.08.046
99. J. Yang, D. Gao, Y. He et al., (2021) in *27th Russian Particle Accelerator Conference*, Status of the hiaf accelerator facility in china doi 10.18429/JACoW-RuPAC2021-TUX01
100. X. Zhou, J. Yang, Status of the high-intensity heavy-ion accelerator facility in china. AAPPS Bull. **32**, 35 (2022). https://doi.org/10.1007/s43673-022-00064-1
101. C. Wilkin, The legacy of the experimental aip conf proc programme at cosy. Eur. Phys. J. A **53**, 114 (2017). https://doi.org/10.1140/epja/i2017-12295-4. arXiv:1611.07250
102. P. Moskal, H.-H. Adam, A. Budzanowski et al., Experimental study of pp η dynamics in the pp → pp η reaction. Phys. Rev. C **69**, 025203 (2004). https://doi.org/10.1103/PhysRevC.69.025203. arXiv:nucl-ex/0307005
103. H. Petren, Chr. Bargholtz, M. Bashkanov et al.,η-meson production in proton-proton collisions at excess energies of 40 and 72 MeV. Phys. Rev. C **82**, 055206 (2010). https://doi.org/10.1103/PhysRevC.82.055206
104. H. Calen, J. Dyring, K. Fransson et al., Measurement of the quasifree pn →pnη reaction near threshold. Phys. Rev. C **58**, 2667–2670 (1998). https://doi.org/10.1103/PhysRevC.58.2667
105. Y. He, H. Jia, H. Cai et al., in *Proc. IPAC'23*, Accelerator driven system - a solution to multiple problems of society. No. 14 in IPAC'23 - 14th International Particle Accelerator Conference, (JACoW Publishing, Geneva, Switzerland, 2023), pp. 5205–5209. https://doi.org/10.18429/JACoW-IPAC2023-FRYG2
106. Z.J. Wang, Y. He, G. Huang et al., in *Proc. 10th International Particle Accelerator Conference (IPAC'19), Melbourne, Australia, 19-24 May 2019*, The Status of CiADS Superconducting LINAC. No. 10 in International Particle Accelerator Conference, (JACoW Publishing, Geneva, Switzerland, 2019), pp. 994–997. https://doi.org/10.18429/JACoW-IPAC2019-MOPTS059
107. S. Liu, W. Chen, W. Dou et al., in *Proc. HIAT'18*, Commissioning of China ADS Demo Linac and Baseline Design of CiADS Project. No. 14 in International Conference on Aip Conf Proc, (JACoW Publishing, Geneva, Switzerland, 2019), pp. 112–116, https://doi.org/10.18429/JACoW-HIAT2018-WEYAA01

108. S. Liu, Z.J. Wang, Y. Tao et al., Physics design of the superconducting section of the ciads linac. Int. J. Mod. Phys. A **34**, 1950178 (2019). https://doi.org/10.1142/S0217751X19501781
109. Z.J. Wang, S.H. Liu, W.L. Chen et al., Beam physics design of a superconducting linac. Phys. Rev. Accel. Beams **27**, 010101 (2024). https://doi.org/10.1103/PhysRevAccelBeams.27.010101
110. H.J. Cai, Y. He, S.H. Liu et al., Towards a high-intensity muon source. Phys. Rev. Accel. Beams **27**, 023403 (2024). https://doi.org/10.1103/PhysRevAccelBeams.27.023403. arXiv:2309.01520
111. R. He, X.Y. Niu, Y. Wang et al., Advances in nuclear detection and readout techniques. Nucl. Sci. Tech. **34**, 205 (2023). https://doi.org/10.1007/s41365-023-01359-0
112. J. Appel, M. Bourquin, I. Gaines et al., Performance of a lead-glass electromagnetic shower detector at fermilab. Nucl. Instrum. Methods **127**, 495–505 (1975). https://doi.org/10.1016/0029-554X(75)90653-9
113. W.P. Ren, W. Zhou, B.H. You et al., Topmetal-M: A novel pixel sensor for compact tracking applications. arXiv:2201.10952, doi 10.1016/j.nima.2020.164557
114. H. Yang et al., Hi'Beam-S: A monolithic silicon pixel sensor-based prototype particle tracking system for HIAF. IEEE Trans. Nucl. Sci. **68**, 2794–2800 (2021). https://doi.org/10.1109/TNS.2021.3128542
115. H.B. Yang, H.L. Zhang, C.S. Gao et al., Heavy-ion beam test of a monolithic silicon pixel sensor with a new 130 nm High-Resistivity CMOS process. Nucl. Instrum. Meth. A **1039**, 167049 (2022). https://doi.org/10.1016/j.nima.2022.167049
116. P. Yang, X.Y. Niu, W. Zhou et al., Design of Nupix-A1, a monolithic active pixel sensor for heavy-ion physics. Nucl. Instrum. Meth. A **1039**, 167019 (2022). https://doi.org/10.1016/j.nima.2022.167019
117. J. Huang, R. He, X. Niu et al., Design of Nupix-A2, a monolithic active pixel sensor for heavy-ion physics. JINST **18**, C11014 (2023). https://doi.org/10.1088/1748-0221/18/11/C11014
118. S. Agostinelli, J. Allison, K. Amako et al., Geant4-a simulation toolkit. Nucl. Instrum. Meth. A **506**, 250–303 (2003). https://doi.org/10.1016/S0168-9002(03)01368-8
119. J. Allison, K. Amako, J. Apostolakis et al., Geant4 developments and applications. IEEE Trans. Nucl. Sci. **53**, 270 (2006). https://doi.org/10.1109/TNS.2006.869826
120. J. Allison, K. Amako, J. Apostolakis et al., Recent developments in Geant4. Nucl. Instrum. Meth. A **835**, 186–225 (2016). https://doi.org/10.1016/j.nima.2016.06.125
121. O. Buss, T. Gaitanos, K. Gallmeister et al., Transport-theoretical description of nuclear reactions. Phys. Rept. **512**, 1–124 (2012). https://doi.org/10.1016/j.physrep.2011.12.001. arXiv:1106.1344
122. Giessen boltzmann-uehling-uhlenbeck project (GIBUU), https://gibuu.hepforge.org/, accessed June 18, 2024
123. T. Gaitanos, H. Lenske, U. Mosel, Fragment formation in proton induced reactions within a BUU transport model. Phys. Lett. B **663**, 197–201 (2008). https://doi.org/10.1016/j.physletb.2008.04.011. arXiv:0712.3292
124. J. Weil, H. van Hees, U. Mosel, Dilepton production in proton-induced reactions at SIS energies with the GiBUU transport model. Eur. Phys. J. A **48**, 111 (2012). https://doi.org/10.1140/epja/i2012-12111-9
125. C. Gatto, G. Blazey, A. Dychkant et al., Preliminary results from ADRIANO2 test beams. Instruments **6**, 49 (2022). https://doi.org/10.3390/instruments6040049
126. G. Battistoni, T. Boehlen, F. Cerutti et al., Overview of the FLUKA code. Ann. Nucl. Energy **82**, 10–18 (2015). https://doi.org/10.1016/j.anucene.2014.11.007
127. Fluka, https://fluka.cern/, accessed June 18, 2024
128. Fluka, http://www.fluka.org/fluka.php, accessed June 18, 2024
129. Q.F. Lü, D.M. Li, Near-threshold η production in pp collisions. Chin. Phys. C **39**, 113104 (2015). https://doi.org/10.1088/1674-1137/39/11/113104. arXiv:1501.06266
130. B. Li, A.T. Sustich, B. Zhang et al., Studies of superdense hadronic matter in a relativistic transport model. Int. J. Mod. Phys. E **10**, 267–352 (2001). https://doi.org/10.1142/S0218301301000575
131. S.A. Bass, M. Belkacem, M. Bleicher et al., Microscopic models for ultrarelativistic heavy ion collisions. Prog. Part. Nucl. Phys. **41**, 255–369 (1998). https://doi.org/10.1016/S0146-6410(98)00058-1. arXiv:nucl-th/9803035
132. M. Bleicher, E. Zabrodin, C. Spieles et al., Relativistic hadron-hadron collisions in the ultrarelativistic quantum molecular dynamics model. J. Phys. G **25**, 1859–1896 (1999). https://doi.org/10.1088/0954-3899/25/9/308. arXiv:hep-ph/9909407
133. M. Bleicher, Ultrarelativistic quantum molecular dynamics (UrQMD)., https://itp.uni-frankfurt.de/~bleicher/index.html?content=urqmd, accessed June 18, 2024
134. M. Al-Turany, D. Bertini, R. Karabowicz et al., The fairroot framework. J. Phys. Conf. Ser. **396**, 022001 (2012). https://doi.org/10.1088/1742-6596/396/2/022001
135. Fairroot, https://fairroot.gsi.de/, accessed June 18, 2024
136. P.H. Adrian, N.A. Baltzell, M. Battaglieri et al., Search for a dark photon in electroproduced e^+e^- pairs with the Heavy Photon Search experiment at JLab. Phys. Rev. D **98**, 091101 (2018). https://doi.org/10.1103/PhysRevD.98.091101. arXiv:1807.11530
137. H. Merkel, P. Achenbach, C. Ayerbe Gayoso et al., Search for light gauge bosons of the dark sector at the mainz microtron. Phys. Rev. Lett. **106**, 251802 (2011). https://doi.org/10.1103/PhysRevLett.106.251802. arXiv:1101.4091
138. S. Giovannella, On behalf of the Kloe-2 Collaboration, U boson searches at KLOE. J. Phys. Conf. Ser. **335**, 012067 (2011). https://doi.org/10.1088/1742-6596/335/1/012067. arXiv:1107.2531
139. J.R. Batley, G. Kalmus, C. Lazzeroni et al., Search for the dark photon in π^0 decays. Phys. Lett. B **746**, 178–185 (2015). https://doi.org/10.1016/j.physletb.2015.04.068. arXiv:1504.00607
140. S. Gninenko, Addendum to the NA64 proposal: Search for the $A' \to$ *invisible* and $X \to e^+e^-$ decays in 2021 (Tech. rep, CERN, Geneva, 2018)
141. E.M. Riordan, M.W. Krasny, K. Lang et al., Search for short-lived axions in an electron-beam-dump experiment. Phys. Rev. Lett. **59**, 755 (1987). https://doi.org/10.1103/PhysRevLett.59.755
142. J. Blumlein, J. Brunner, New exclusion limits for dark gauge forces from beam-dump data. Phys. Lett. B **701**, 155–159 (2011). https://doi.org/10.1016/j.physletb.2011.05.046. arXiv:1104.2747
143. J. Blümlein, J. Brunner, New exclusion limits on dark gauge forces from proton bremsstrahlung in beam-dump data. Phys. Lett. B **731**, 320–326 (2014). https://doi.org/10.1016/j.physletb.2014.02.029. arXiv:1311.3870
144. S.N. Gninenko, Constraints on sub-GeV hidden sector gauge bosons from a search for heavy neutrino decays. Phys. Lett. B **713**, 244–248 (2012). https://doi.org/10.1016/j.physletb.2012.06.002. arXiv:1204.3583
145. P.H. Adrian, N.A. Baltzell, M. Battaglieri et al., Searching for prompt and long-lived dark photons in electroproduced e+e- pairs with the heavy photon search experiment at JLAB. Phys. Rev. D **108**, 012015 (2023). https://doi.org/10.1103/PhysRevD.108.012015. arXiv:2212.10629
146. S. Abrahamyan, Z. Ahmed, K. Allada et al., Search for a new gauge boson in electron-nucleus fixed-target scattering by the apex experiment. Phys. Rev. Lett. **107**, 191804 (2011). https://doi.org/10.1103/PhysRevLett.107.191804. arXiv:1108.2750
147. J.D. Bjorken, R. Essig, P. Schuster et al., New fixed-target experiments to search for dark gauge forces. Phys. Rev. D **80**, 075018

(2009). https://doi.org/10.1103/PhysRevD.80.075018. arXiv:0906.0580
148. L. Marsicano, M. Battaglieri, M. Bondi' et al., Dark photon production through mater sci forum in beam-dump experiments. Phys. Rev. D **98**, 015031 (2018). https://doi.org/10.1103/PhysRevD.98.015031. arXiv:1802.03794
149. B. Batell, R. Essig, Z. Surujon, Strong constraints on sub-GeV dark sectors from slac beam dump E137. Phys. Rev. Lett. **113**, 171802 (2014). https://doi.org/10.1103/PhysRevLett.113.171802. arXiv:1406.2698
150. J.D. Bjorken, S. Ecklund, W.R. Nelson et al., Search for neutral metastable penetrating particles produced in the slac beam dump. Phys. Rev. D **38**, 3375 (1988). https://doi.org/10.1103/PhysRevD.38.3375
151. M. Ablikim, M. N. Achasov, X.C. Ai et al., Amplitude analysis of the decays $\eta' \to \pi^+\pi^-\pi^0$ and $\eta' \to \pi^0\pi^0\pi^0$. Phys. Rev. Lett. **118**, 012001 (2017). https://doi.org/10.1103/PhysRevLett.118.012001. arXiv:1606.03847
152. B.M.K. Nefkens, S. Prakhov, P. Aguar-Bartolomé et al., New measurement of the rare decay $\eta \to \pi^0\gamma\gamma$ with the crystal ball/taps detectors at the mainz microtron. Phys. Rev. C **90**, 025206 (2014). https://doi.org/10.1103/PhysRevC.90.025206. arXiv:1405.4904
153. F. Bergsma, J. Dorenbosch, J.V. Allaby et al., Search for axion like particle production in 400-GeV proton-copper interactions. Phys. Lett. B **157**, 458–462 (1985). https://doi.org/10.1016/0370-2693(85)90400-9
154. Y.S. Liu, I.C. Cloët, G.A. Miller, Eta decay and muonic puzzles. Nucl. Phys. B **944**, 114638 (2019). https://doi.org/10.1016/j.nuclphysb.2019.114638
155. R. Bilger, W. Brodowski, H. Calén et al., Measurement of the pd $\to^3$He η cross-section between 930-MeV and 1100-MeV. Phys. Rev. C **65**, 044608 (2002). https://doi.org/10.1103/PhysRevC.65.044608
156. J. Smyrski, H.-H. Adam, A. Budzanowski et al., Measurement of the dp $\to^3$He η reaction near threshold. Phys. Lett. B **649**, 258–262 (2007). https://doi.org/10.1016/j.physletb.2007.04.021. arXiv:nucl-ex/0702043
157. T. Mersmann, A. Khouka, M. Büscher et al., Precision study of the η He-3 system using the dp $\to$ He-3 η reaction. Phys. Rev. Lett. **98**, 242301 (2007). https://doi.org/10.1103/PhysRevLett.98.242301. arXiv:nucl-ex/0701072
158. T. Rausmann, A. Khoukaz, M. Büscher et al., Precision study of the dp $\to$ ^{3}He η reaction for excess energies between 20 MeV and 60 MeV. Phys. Rev. C **80**, 017001 (2009). https://doi.org/10.1103/PhysRevC.80.017001. arXiv:0905.4595
159. P. Adlarson, W. Augustyniak, W. Bardan et al., Cross section ratio and angular distributions of the reaction p + d $\to^3$He + η at 48.8 MeV and 59.8 MeV excess energy. Eur. Phys. J. A **50**, 100 (2014). https://doi.org/10.1140/epja/i2014-14100-4. arXiv:1402.3469